Coastal Engineering 161 (2020) 103768

Contents lists available at ScienceDirect

Coastal Engineering

journal homepage: www.elsevier.com/locate/coastaleng

Sandbar dynamics in microtidal environments: Migration patterns in unprotected and bounded beaches

Lorenzo Melito [a,*], Luca Parlagreco [b], Eleonora Perugini [a], Matteo Postacchini [a], Saverio Devoti [b], Luciano Soldini [a], Gianluca Zitti [a], Luca Liberti [b], Maurizio Brocchini [a]

[a] Department of Civil Engineering and Architecture (DICEA), Università Politecnica delle Marche, Ancona, Italy
[b] Italian Institute for Environmental Protection and Research (ISPRA), Rome, Italy

ARTICLE INFO

Keywords:
Sandbars
Net offshore migration
Oscillation around a point of equilibrium
Beachface
Beach morphodynamics

ABSTRACT

Novel observations of bar features and migration patterns at three Italian sandy beaches in Senigallia (central Adriatic Sea) and Terracina (central Tyrrhenian Sea) are presented. While two of these beaches are unprotected, one is artificially embayed through the presence of a concrete jetty. Bar locations and motions are analysed with video imagery data sets from coastal monitoring stations. Wave climate from the Copernicus oceanographic model is used to correlate hydrodynamics and beach morphology. Clear net offshore migration (NOM) patterns are identified at all beaches, although exhibiting different response scales. At the low-slope beach of Senigallia (mean surf zone slope of 0.009) bars are more sensitive to seasonal changes in wave climate, with offshore shifts in winter and inactivity in summer. Mean annual migration rates of up to 0.26 m/day and 0.09 m/day are observed for outer and inner bars, respectively. No significant response to single storms is observed, except during a single NNE storm. No distinct erosive or accretive trend for the shoreline is evidenced. At the steep beach of Terracina (mean surf zone slope of 0.018), conversely, bars are strongly responsive to single storm events, with displacements of up to 25–50 m across a single storm. The mean inter-annual migration rate is 0.08 m/day for the single/outer bar, whereas a slight onshore trend (-0.02 m/day) for the newborn inner bar is established. The presence of an artificial jetty at the Misa river mouth in Senigallia, finally, leaves the bar system, typically oscillating around an equilibrium position, susceptible to larger seasonal oscillations and strong offshore migration due to two ESE storm events. Numerical simulations of nearshore circulation for two storms from different directions predict the birth of longshore currents, higher ratios of significant wave height to water depth, and stronger bottom orbital velocities over bars in case of the ESE storm, suggesting a greater tendency for offshore-directed sediment transport.

1. Introduction

Sandy beaches in wave-dominated coasts frequently feature sand bars (Wijnberg and Kroon, 2002). Generated in various shapes and sizes, they are the product of converging patterns of sediment transport induced by complex hydrodynamic processes in the surf zone (Roelvink and Stive, 1989). Bars serve as preferential points of wave energy dissipation through breaking (Lippmann and Holman, 1989), and are thus a primary form of beach protection and have strong implications on both short- and long-term coast stability, beach erosion and shoreline changes (Phillips et al., 2017; Angnuureng et al., 2017).

The location of sandbars changes over time in response to the variability of the offshore wave climate. It is consolidated that, in the short term, bars tend to migrate offshore under breaking waves and very energetic wave conditions (Gallagher et al., 1998; Ruessink and Terwindt, 2000). Seaward migration has been linked to the development of strong mid-water, offshore-directed currents (undertow) driven by wave breaking over bar crests. Such currents carry sediment towards the sea and move the bar offshore (Gallagher et al., 1998). Onshore bar motion, on the other hand, is often observed under non-breaking waves and fairly intense wave climate (Sunamura and Takeda, 1984; Hoefel and Elgar, 2003), although onshore migration under storm conditions have been evidenced in some studies (Aagaard et al., 1998; Houser and Greenwood, 2007). Mechanisms of onshore bar migration are still debated. It is argued that a significant role in this phenomenon is played by (landward) asymmetries in fluid acceleration and velocity under the steep wave front of shoaling waves, promoting sediment entrainment and a shoreward transport (Hoefel and Elgar, 2003; Fernández-Mora et al., 2015).

* Corresponding author.
E-mail address: l.melito@univpm.it (L. Melito).

https://doi.org/10.1016/j.coastaleng.2020.103768
Received 28 March 2020; Received in revised form 15 June 2020; Accepted 27 July 2020
Available online 29 July 2020

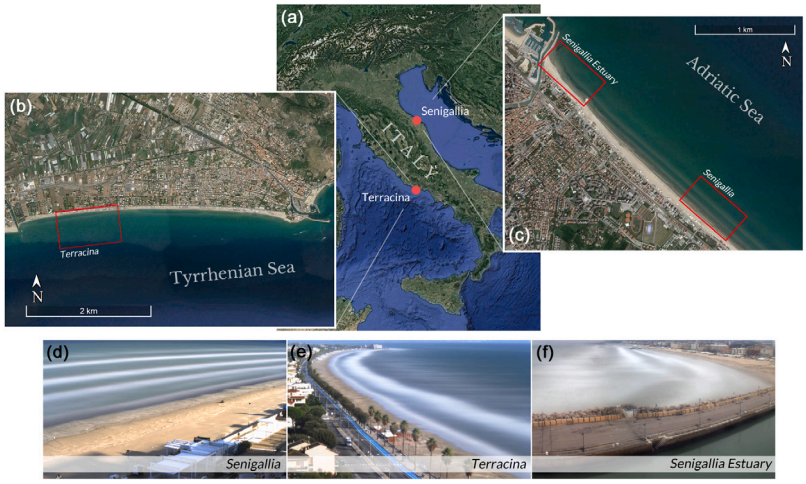

Fig. 1. (a) Map of Italy and locations of Senigallia and Terracina. (b) Location of the video-monitored beach of *Terracina*. (c) Locations of the video-monitored beaches of *Senigallia Estuary* and *Senigallia*. The bottom panels show examples of timex pictures used for the identification of bar crest locations at (d) *Senigallia*, (e) *Terracina*, and (f) *Senigallia Estuary*.

Since the seminal contribution of Wright and Short (1984), a growing body of literature has been devoted to understand the dynamics of bar systems and their connection to wave action, either by using bathymetric surveys (e.g., see Ruessink and Kroon, 1994; Wijnberg and Terwindt, 1995; Sénéchal et al., 2009), or analytical and numerical models (e.g., see Plant et al., 1999; Masselink, 2004; Walstra et al., 2016). Recent years have seen a boost in the employment of remote sensing techniques to overview large portions of coasts and track bar positions and motions through time-exposure imagery (e.g., see Lippmann and Holman, 1990; van Enckevort and Ruessink, 2003; Ruessink et al., 2009).

Some conceptual models have been proposed to describe the morphology and behaviour of sandbars (Brocchini, 2019). In the widely recognized Net Offshore Migration (NOM) model, a sand bar undergoes a three-stage cycle often spanning years to decades. The bar is firstly generated close to the shore (Roelvink and Stive, 1989); then it migrates offshore in response to intense wave conditions (Gallagher et al., 1998); finally, it degenerates and eventually disappears in the outer nearshore (Wijnberg, 1997). Alternatively, the Net Onshore Migration (NOnM) model suggests that sandbars are generated near the breakpoint and migrate towards the shore as a result of dominant onshore sediment transport due to wave skewness during storms (Aagaard et al., 2004). Finally, in opposition to the NOM and NOnM models, the Oscillation around a Point of Equilibrium (OPE) model applies whenever a bar oscillates around a long-term equilibrium position regardless of the incoming wave energy (Certain and Barusseau, 2005).

NOM cycles at time scales of years to decades have been observed on microtidal-to-mesotidal coasts in the Netherlands (Ruessink and Kroon, 1994; Wijnberg and Terwindt, 1995), USA (Birkemeier, 1985; Lippmann et al., 1993), New Zealand (Shand and Bailey, 1999), Australia (Ruessink et al., 2009) and Japan (Kuriyama, 2002). On the other hand, occurrences of systematic NOnM cycles across decades have been reported along the Danish coast of Skallingen (Aagaard et al., 2004).

Notwithstanding the importance of submerged bars in the protection of coastal environments, only a few studies have been performed so far on Mediterranean barred beaches, often characterized by low tidal ranges. NOM cycles with different migration rates and characteristics have been observed across several study sites in the Gulf of Lions, France (Aleman et al., 2013), suggesting that the development of NOM patterns may be dependent on environmental parameters like shore slope, sediment budget and coastal structures. In Séte, France (Certain and Barusseau, 2005), on the other hand, a dominant OPE behaviour is documented at both seasonal and multiannual scale for the inner bar, although a significant storm event caused a strong offshore migration of the outer bar and subsequently triggered a NOM cycle with a time scale of a few years. Armaroli and Ciavola (2011) studied the unprotected portion of Lido di Dante beach (Italy) and conversely observed very limited cross-shore motions of the bars, with no sign of NOM behaviour.

This paper presents a novel set of observations of bar morphology and patterns along three microtidal Italian coasts: (i) the coastal zone close to the mouth of the Misa River (Senigallia, central Adriatic Sea), where the bar system is adjacent to a concrete river jetty; (ii) the touristic coastline a few kilometres south of such estuary, where the sand bar system evolves unbounded by surrounding artefacts; (iii) the coast of Terracina (central Tyrrhenian Sea). Migration patterns are discussed in conjunction with the dominant wave climate, obtained from the Mediterranean Sea Waves wave model by the E.U. Copernicus Marine Service. This study contributes in expanding the knowledge of video-sensed bar displacement features in microtidal beaches, which we believe are under-represented in the scientific literature as of today.

A brief description of the investigated beaches and the employed technology and methods is given in Section 2. A detailed description of bar migration features for the three field sites is given in Section 3. The results are discussed in Section 4 and concluding remarks are provided in Section 5.

2. Materials and methods

2.1. Field sites

The coast of Senigallia, along the Adriatic Sea in central Italy (Fig. 1a and c), is located in a microtidal environment, with semidiurnal tide, a tidal range rarely exceeding 0.6 m and negligible tidal currents. The coastline has a NW–SE orientation and faces approximately 40° from the north. The submerged beach is characterized by fine-to-medium sands with a median grain size (d_{50}) of 0.125–0.25 mm (Postacchini et al., 2017), a beach face slope of 0.025–0.035, a mean surf zone slope of 0.009, and a lower beach slope of 0.001–0.005. This sandy beach usually features an array of three–four shore-parallel, shallow bars within 400 m from the shoreline, in water depths between 0 and 3 m (Fig. 2). A study of medium-term coastal dynamics in the area has shown that differences in storm directionality and intensity induce year-specific net seaward as well as landward bar migration (Postacchini et al., 2017). Two portions of the coastline, with different characteristics in terms of coastal boundaries, are investigated in this work: (i) the 500 m-long stretch of beach adjacent to the engineered Misa river mouth, delimited by the river jetty to the north and the pier of the Rotonda a Mare to the south (*Senigallia Estuary* hereinafter; Fig. 1c and f), and (ii) the unprotected touristic beach around 2 km south of the Misa river estuary, where no man-made coastal

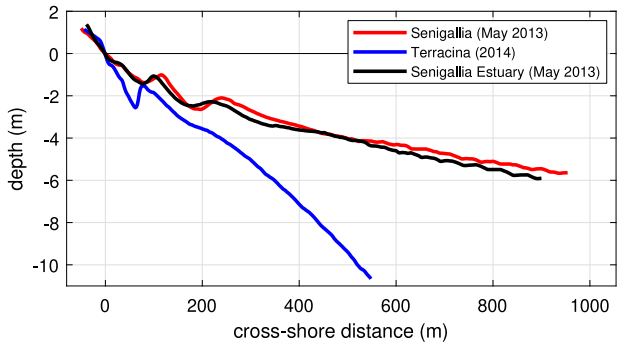

Fig. 2. Representative vertical profiles for the beaches of *Senigallia* (May 2013; red line), *Terracina* (2014; blue line) and *Senigallia Estuary* (May 2013; black line). (For interpretation of the references to colour in this figure legend, the reader is referred to the web version of this article.)

structures interfere with the beach morphology (*Senigallia* hereinafter; Fig. 1c and d). Both beaches present very similar characteristics in regard to mean bottom slopes, locations and shapes of underwater bars (see red and black profiles in Fig. 2).

The Terracina beach (*Terracina* hereinafter) is located along the Tyrrhenian side of central Italy (Fig. 1a–b) and is representative of a 15 km-long embayment with an approximate W–E orientation, delimited by the Circeo headland to the western end. The coastline faces approximately 170° from the north. The tidal regime in the area is microtidal and semidiurnal, with a tide excursion lower than 0.4 m (Evangelista et al., 2004). The beach face features a steep slope of 0.04–0.06 and the mean surf zone slope is 0.018, while the lower beach has a mean slope of 0.02. This coast usually presents a single or double bar configuration with rather steep bars (blue profile in Fig. 2). Native beach sediments consisted of fine-to-medium sands (d_{50} = 0.3 mm), but later shifted to mixed-beach sediments after a beach face nourishment with a mean infill of 270 m^3/m was performed in 2007. Parlagreco et al. (2011) discussed the beach response to the nourishment and observed an initial reorganization of sediment into a single-bar morphology which later evolved into a double-bar system. The inner bar often features slight crescentic patterns in mild climate (Fig. 1e) and is occasionally straightened by the action of storm waves (Parlagreco et al., 2011).

All beaches are considered as intermediate-to-dissipative according to the classification system by Wright and Short (1984).

2.2. Wave data and storms statistics

A 13-year wave hindcast from the Mediterranean Sea Waves oceanographic model by the E.U. Copernicus Marine Service (CMEMS) (Korres et al., 2019) has been used to gather information on wave climate, to make up for the lack of wave buoys for in-situ observations. Spectral wave heights and mean periods are reasonably well estimated by the model (with a typical difference of 0.23 m for the significant wave height and 0.69 s for the mean wave period in the whole Mediterranean Sea; the reader is referred to the quality information document of the hindcast model for further details Zacharioudaki et al., 2019), so we could assume modelled outputs as reliable data for the following analysis. Although we recognize that recent studies have brought into question the capability of global hindcast models to correctly predict accurate values for mean wave direction, especially for strongly oblique waves (de Swart et al., 2020), we deemed reasonable to adopt hindcast outputs also for wave direction, since the wave directionality as modelled by the Copernicus model is highly consistent with the typical observed wave climate experienced by all the investigated beaches.

Hourly-averaged values of significant wave height H_s, peak period T_p, and main wave direction θ have been collected at the closest model nodes to the investigated beaches (at a water depth of around 10.5 m for *Senigallia* and *Senigallia Estuary*, and around 13.5 m for *Terracina*), to limit data spreading in wave directionality. In view of their proximity, only 2 km apart, it has also been assumed that the Adriatic sites of *Senigallia* and *Senigallia Estuary* are subjected to the same wave regime, thus the same wave climate data set has been used for both locations for the rest of our study.

Wave climate statistics and directional roses for both locations are shown in Fig. 3. The wave climate along the Adriatic sites of *Senigallia* and *Senigallia Estuary* is dominated by sea and swell waves with an annual average significant wave height H_s of 0.44 m and peak period T_p of 4.1 s. The largest waves (H_s > 0.75 m) are generated during Bora storms and approach from NNE, even though energetic Scirocco-driven waves from eastern directions are frequently observed (Fig. 3a). *Terracina*, on the Tyrrhenian side, is mainly subjected to regular swell waves with an annual average H_s of 0.38 m and T_p of 5.1 s. The coast is typically exposed to waves with high obliquity, with about half of the total wave records approaching from SSW over the period 2015–2018, although a fraction of relevant waves with H_s > 1 m comes also from SE (Fig. 3b). The slightly shorter average period and higher average wave heights for *Senigallia* are due to shorter fetch distances available in the Adriatic sea, which lead to limited swell intensity in favour of steep wind-generated waves, especially from northern quadrants. Wave climates at both locations show a marked seasonal variability, with monthly averaged H_s of 0.2–0.4 m during summer and up to 0.7 m in winter (Fig. 3c).

Hourly wave climate records have been processed to identify significant storm events. Although H_s exceedance values of 5%–10% are commonly used thresholds for the definition of storm events (Splinter et al., 2014), an even stricter exceedance threshold of 3% of the whole H_s available data set (2006–2018) has been used here to single out storms with higher impact potential. A proper storm event has been then defined whenever the hourly value of H_s exceeded the assumed threshold for more than 12 consecutive hours. Following Boccotti (2000), a storm event has been regarded as independent if separated from the previous and following ones by a continuous interval of more than 12 h. Two storms have been merged to form a single storm event whenever they were separated by less than 12 h.

Once a set of classified storms has been defined, the wave energy flux of each storm (per unit of wave-crest length) F has been computed as (Tucker and Pitt, 2001):

$$F = E\,c_g = \frac{\rho g^2}{64\pi} H_s^2\,T_p, \tag{1}$$

where $E = \frac{\rho g H_s^2}{16}$ is wave energy for random waves, $c_g = \frac{gT_p}{4\pi}$ is the group celerity in the assumptions of deep water and linear wave theory, ρ is water density (set at a standard value of 1026 kg/m^3) and g is the acceleration due to gravity. The cross-shore and alongshore components of the energy flux (per unit length of beach), F_x and F_y, are calculated as:

$$F_x = F\cos^2\theta_m, \tag{2}$$

$$F_y = F\sin\theta_m\cos\theta_m, \tag{3}$$

where θ_m is the wave direction with respect to the shore normal. For each classified storm, the total energy flux has been computed as the sum of energy fluxes of each storm hour. Additionally, weekly values of cumulated wave energy have been evaluated by summing hourly values of E across each week.

2.3. Video-monitoring analysis and products

Daily average locations for shorelines and bar crests have been extracted from video imagery collected by monitoring stations nearby the investigated areas.

The *Senigallia Estuary* beach is monitored by the Sena Gallica Speculator (SGS) station, deployed at the Senigallia harbour within the

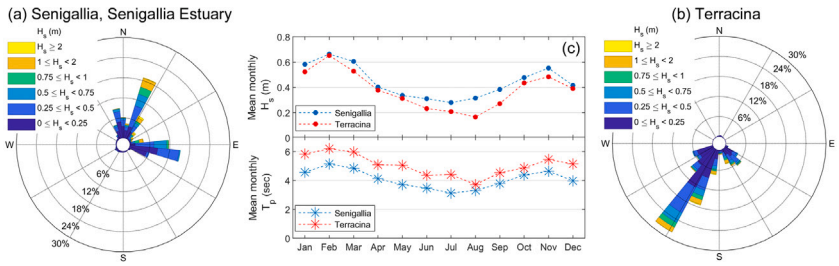

Fig. 3. Directional wave roses for (a) *Senigallia* and *Senigallia Estuary*, and (b) *Terracina*, showing the directional distribution of H_s across the period 2015–2018. (c) Monthly mean statistics of H_s and T_p over the period 2015–2018.

EStuarine COhesive SEDiments (EsCoSed) project framework (Brocchini et al., 2017). The station is composed of four cameras located on the top of a tower, 25 m above the mean sea level, and oriented to encompass both the estuary of the Misa River and the 500 m-long stretch of unprotected beach adjacent to the southern jetty, with an overall field-of-view angle of around 200° (Fig. 1f). The nearshore regions of *Senigallia* and *Terracina* are monitored by video systems deployed and maintained by the Italian Institute for Environmental Protection and Research (ISPRA)[1] in the context of the COastal Protection and resiliEnce MApping in Protected areas (CoPEMaP) project (Parlagreco et al., 2019). The monitoring stations are located more than 20 m above the mean sea level and less than 150 m from the shoreline, collecting images of the nearshore zone (800 m and 500 m in the along-shore and cross-shore direction, respectively; Fig. 1d–e) at 2 Hz for ten minutes in each daylight hour through a double digital video-camera.

The collected images have been hourly averaged, orthorectified and stabilized to obtain time exposure (timex) images. Transient features, like individual waves, are removed from timex images, whereas white regions appear at locations of preferential wave breaking; such regions are used as proxies for the location of bar crests and shorelines (Lippmann and Holman, 1990; Holman et al., 1993). Fig. 1d–f shows examples of identified bar lines and shorelines, appearing as regions of high pixel intensity, for the three study sites. The Barline Intensity Mapper (BLIM) semi-automatic algorithm has been used to identify shoreline and bar locations (van Enckevort and Ruessink, 2003). To the purpose of bar/shoreline identification, the analysed portions of each rectified image have been fixed at a distance from the stations where pixel footprints were not higher than 5 m and 20 m in the cross-shore and alongshore direction, respectively.

Mild climates often hinder bar detection due to lack of wave breaking. On the other hand, very high waves and a low-sloping or flat bathymetry often lead to wave breaking over a wider cross-shore region, thus making the identification of a single, reliable bar crest location unclear. To comply with these restrictions, a single timex image per day has been selected with the best environmental conditions to clearly identify bar locations with low uncertainty. Although it is well-known that differences in water level due to tidal excursion may cause artificial shifts of the breaker line (e.g., see van Enckevort and Ruessink, 2001), the effect of tide on bar crest identification has not been considered in this work, due to the low tidal ranges typical of the investigated beaches. Furthermore, images in which sand bar locations could not be identified due to poor image quality, system malfunctioning or mild waves have been discarded. In conclusion, a total of 786, 454 and 1176 images have been processed to identify morphological features in *Senigallia*, *Senigallia Estuary*, and *Terracina*, respectively.

The detected position of each sand bar and shoreline has been finally averaged in the alongshore direction to obtain a single mean cross-shore position per day, given with respect to local reference systems. *Senigallia* and *Terracina* bars present a good alongshore uniformity, with limited or absent crescentic shapes (Fig. 1d and e); this setting makes the definition of a single alongshore-averaged cross-shore bar position suitable. In *Senigallia Estuary* (Fig. 1f) bar lines tend to follow the curvature of the embayed beach, making the evaluation of the mean position of the whole bar somewhat inaccurate. In order to avoid such inaccuracy, the average position of only the central 200 m of each bar line has been evaluated.

Multi-annual, seasonal and weekly components of migration patterns for bars and shorelines have been extracted from bar position time series, with a method similar to that adopted by van Enckevort and Ruessink (2003). The time series of cross-shore feature position has been first filtered with a Savitzky–Golay filter with a window half-length of one year (365 days) in order to obtain its inter-annual component. The residual (i.e., the difference between the original time series and the inter-annual component) has been filtered again with a window half-length of three months (90 days) to get the seasonal trend of the data. The ultimate residual is finally filtered with a window half-length of one week (7 days) to obtain weekly trends. Inter-annual migration rates have been calculated as time derivatives of the inter-annual component. Similarly, seasonal migration rates have been evaluated as time derivatives of the sum of inter-annual and seasonal components, and calculated separately for summer and winter seasons.

2.4. Numerical modelling and potential for sediment motion at Senigallia Estuary

The presence of rigid coastal structures at *Senigallia Estuary* (Section 3.3) is likely to have an impact on the hydrodynamic features and, accordingly, on the morphology of the area. In view of this, a characterization of nearshore circulation in the region close to the river pier has been made by use of the numerical solver FUNWAVE (Shi et al., 2012) in an attempt to shed some light on the processes leading to bar migration in the embayed beach of *Senigallia Estuary*.

FUNWAVE is a widely used non-linear, phase-resolving wave model based on the Boussinesq equations, best suited to describe propagation of long waves over intermediate-to-shallow water. Its applicability to swash and inner surf zones has been recently improved as processes typically occurring in very shallow waters (wave breaking, bore propagation, wave runup) are modelled by locally switching to a Non-linear Shallow Water (NSWE) solver upon exceedance of a certain Froude number threshold.

A proper modelling of circulation patterns through numerical solvers requires an adequate description of the bathymetry in the region of interest. Unfortunately, recent extensive bathymetric data are not available for the area, thus the exact morphology in place in the period when bar crest observations have been taken (from July 2015 to March 2019) could not be modelled and tested. Numerical simulations, still representative of the typical dynamics of the area, have been nonetheless made with the most recent DTM data set available for the region (2013). The DTM presents two well-formed (middle and outer) bars, at about 2 m and 1 m depth, respectively (red dots in Fig. 4). The middle bar extends well near the estuary jetty in a curved fashion. Hints

[1] http://videomonitoraggio.isprambiente.it.

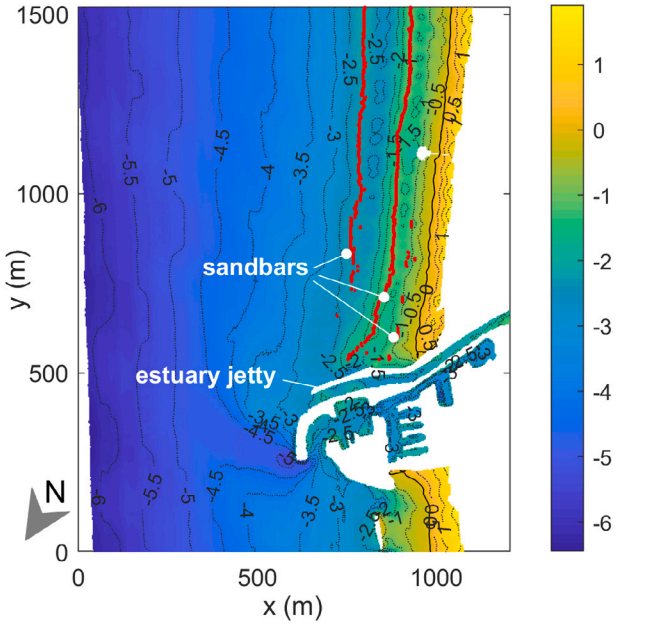

Fig. 4. Numerical domain used in the simulations. Bathymetry contours are shown in dotted grey lines. The shoreline is shown by the thick contour at $z = 0$ m. The estuary jetty is labelled, as well as the DTM bars (also highlighted by red dots).

of a less apparent inner formation can still be detected at about 0.5–1 m depth. The hydrodynamics modelled on such bathymetry, therefore, can be taken as representative of circulation features occurring in the presence of underwater bars.

The DTM has been converted into a rectangular grid with regular spacing ($\delta x = \delta y = 2.5$ m) covering the nearshore region of Senigallia Estuary up until about 6 m depth. The emerged regions 1.5 m above the water level and the rigid structures (estuary jetties, harbour facilities; white areas in Fig. 4) have been made impermeable and reflective, while the lateral boundaries (the top and bottom sides of the domain in Fig. 4) have been set as transparent, to avoid undesired wave reflections at the borders of the domain. The longshore and cross-shore extensions of the effective grid are 1.5 km and 1.2 km, respectively.

Two numerical simulations have been conceived to inspect differences in the hydrodynamics generated by storms events approaching from the two main wave attack directions in *Senigallia Estuary*: ESE for Scirocco storms, and NNE for Bora storms. JONSWAP spectra have been used as wave inputs at a water depth of about 6 m. To simulate the impact of a typical ESE storm, storm-averaged and peak wave parameters from the February 28–29, 2016 storm event ($H_{s,mean}$ = 2.26 m, T_p = 9.3 s and $\theta_{mean} = -15°$ with respect to the offshore boundary) have been given as input. For the simulation of a NNE storm, parameters from the March 22–24, 2016 storm ($H_{s,mean}$ = 2.28 m, T_p = 7.6 s and $\theta_{mean} = 12°$ with respect to the offshore boundary) have been chosen as input. The simulations were run for 6 model hours.

Representative 30-minute-averaged fields of depth-averaged velocity U and significant wave height H_s at the last simulated hour have been extracted from numerical outputs. Additionally, the wave-induced root-mean-square bottom orbital velocity U_{rms} has been evaluated from the field of H_s according to the empirical formulation by (Soulsby and Smallman, 1986):

$$U_{rms} = \frac{H_s}{T_n} \frac{0.25}{(1 + A\,t^2)^3}, \tag{4}$$

$$A = \left[6500 + (0.56 + 15.54\,t)^6\right]^{1/6}, \tag{5}$$

where $t = T_n/T_z$. $T_n = (d/g)^{1/2}$ is a natural scale for wave periods and T_z is the average zero-crossing period, which can be estimated from the peak period T_p for a JONSWAP spectrum as $T_z = T_p/1.281$. In order to evaluate the potential for sediment mobilization, U_{rms} has been compared with the critical bottom velocity for sediment motion U_{cr}, evaluated after (Soulsby, 1997; Komar and Miller, 1973):

$$U_{cr} = \left[0.118\,g\left(\frac{\rho_s}{\rho} - 1\right)\right]^{2/3} d_{50}^{1/3}\,T_p^{1/3}. \tag{6}$$

Table 1
Mean inter-annual and seasonal migration rates for the morphological features in *Senigallia* shown in Fig. 7. Positive (negative) values indicate offshore (onshore) migration.

Feature	Mean interannual m/day	Seasonal (summer) m/day	Seasonal (winter) m/day
b1 (inner)	0.09	−0.15	0.2 – 0.25
b2 (middle)	0.19	0 – 0.1	0.4 – 0.45
b3 (outer)	0.26	0.05 – 0.15	0.3 – 1
b5 (inner)	0.06	−0.1 – 0	0 – 0.25
Shoreline	−0.008	–	–

3. Results

Bar migration patterns and their relationships with wave climate are discussed in this section. To better explain similarities and contrasts in coastal dynamics for the three investigated beaches, observations for the two beaches that are not influenced by man-made structures, *Senigallia* and *Terracina*, are presented first. Afterwards, the dynamics at the beach of *Senigallia Estuary*, bounded by the river jetty and the Rotonda pier, are discussed.

3.1. Senigallia

Fig. 5 shows morphological and wave data for the beach of *Senigallia* between December 2016 and January 2019.

The submerged beach is characterized by 3 to 4 bars presenting an inter-annual trend of offshore migration (Fig. 5d). Bar migration appears to be more related to seasonal changes in wave climate, with enhanced offshore migration in winter climate (September to March) and bar inactivity or very mild onshore migration during summer months. This is confirmed by the outermost bars (*b2* and *b3*; red and grey dots in Fig. 5d) exhibiting a total offshore migration of as much as 50 m and 100 m respectively across 2017.

Storm-event response is strikingly absent. The most significant change in bar setting is nonetheless driven by a major, long-lasting NNE (Bora) storm event in February 2018, that triggers a large offshore migration of outer bar *b5* (approximately 40 m across five days) and minor displacement of 10–15 m for inner bars *b1* and *b2*.

The winter season 2017–2018 is characterized by the gradual generation and detachment of a new inner bar *b5* that matches the gradual offshore migration and decay of the outermost bar *b3*. Although some manifestation of the new bar feature could be traced back to the beginning of the winter season, in the form of sub-parallel formations occasionally welding to the shoreline (see Fig. 6a–b for examples of sub-parallel bar fragments in November 2017), visual inspection of the timex allowed us to assess the first proper evidence of the new sand formation after the 54-hour storm event in October 2017. For several weeks after this storm, the newborn bar was visible in timex images as an additional breaking region very close to the shoreline during high tide, and occasionally emerged in low tide because of its shallow depth. The shoreline gradually migrating offshore across the winter season 2017–2018 is, as a matter of fact, the new inner bar (identified as the most landward breaking region) slowly detaching from the upper beach face to form a proper subtidal feature (Fig. 6c).

In the following year (2018) the new bar system followed the same behaviour of the previous year, with a relative stability in summer and increased offshore migration in winter. The shoreline appears to be stable and no erosive or accretive trends are identified.

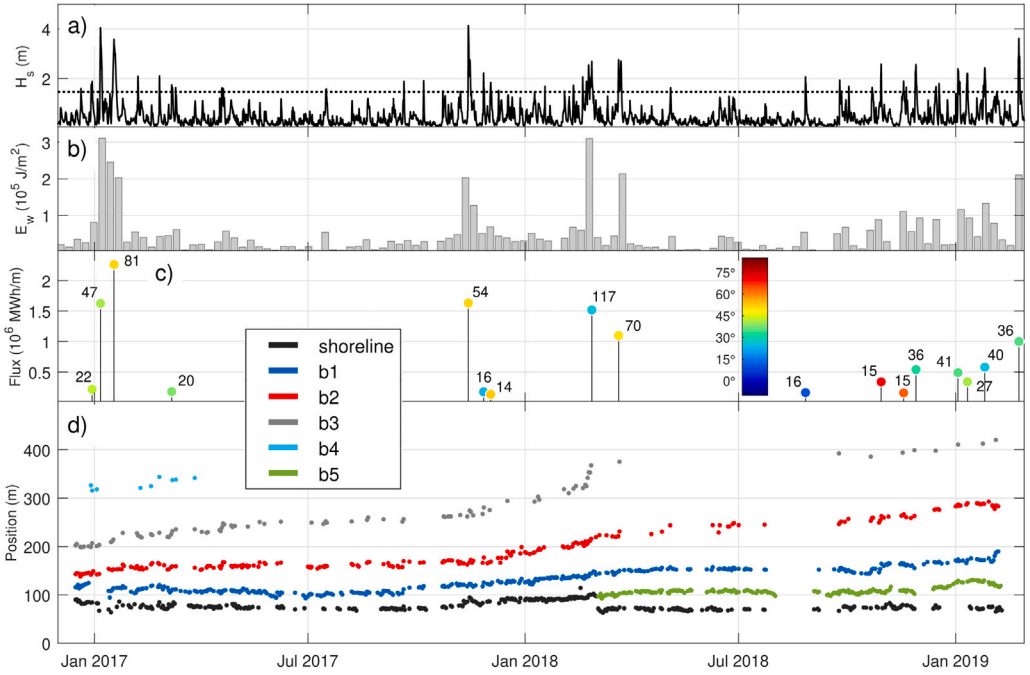

Fig. 5. Wave climate and bar configuration in *Senigallia* (December 2016–January 2019). (a) Modelled offshore significant wave height (solid line) and storm threshold (dashed line). (b) Cumulated weekly wave energy. (c) Characterization of classified storms. Stems length represents the energy flux. Numbers represent storm duration (in hours). Marker colours indicate the peak storm wave direction (°N). (d) Cross-shore, alongshore-averaged bar and shoreline position. (For interpretation of the references to colour in this figure legend, the reader is referred to the web version of this article.)

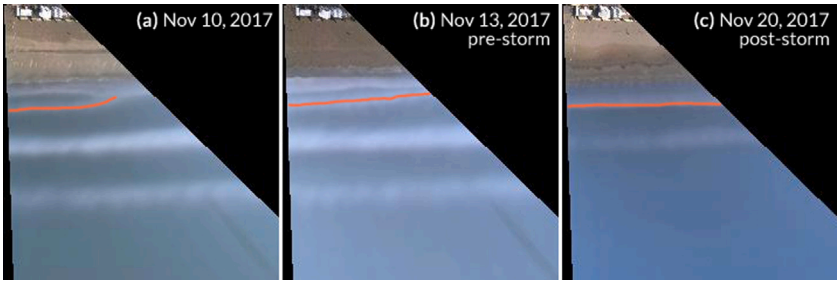

Fig. 6. Detachment and definition of inner bar *b5* (orange lines) in *Senigallia* in November 10–20, 2017. (a) (b) The sub-parallel bar appears as a breaking region and occasionally welds to the shoreline. (c) The bar becomes parallel to the shore after the November 13–15, 2017 storm.

The extracted trends are presented in Fig. 7 for each identified morphological feature. Fig. 7 confirms the presence of well-defined, offshore-directed yearly trends (with mean inter-annual migration rates of as much as 0.26 m/day for the outer bar *b3* and 0.06–0.09 m/day for inner bars *b1* and *b5*; Table 1) superimposed with strong seasonal signals (onshore-directed or stable in summer months and offshore-directed in winter months) for all features. The mean shoreline position presents inter-annual stability in spite of the bar generation process occurring in winter 2017–2018, suggesting that the new bar development happened at no expenses on the total sediment budget of the beach.

3.2. Terracina

Fig. 8 displays morphologic and wave data for the beach of *Terracina* in the period October 2015–December 2018. The double-barred system shows global seaward displacement in winter climate and general stability or mild onshore migration in summer. Unlike in *Senigallia* (Section 3.1), though, frequent bar displacements in the order of 25–50 m are also observed in response to single storm events, causing an overall seaward migration across a single season.

A 50 m net offshore migration of bar *b1* is observed in the winter season 2016–2017 as the consequence of a series of mildly energetic but short-lived storms, with each event exceeding the H_s threshold for around one day only. In the following summer season the bar recovered by slightly moving onshore with very mild wave climate.

A strong offshore migration happened again at the end of 2017, when a group of southern storms triggered a net 50 m offshore migration of bar *b1*, along with the generation of a new inner bar *b3* and a shoreline retreat of 10 m (Fig. 8d). The new 2-bar configuration is effective in protecting the coast against the intense stormy state that follows (February–April 2018), with both bars moving back and forth around their new equilibrium points, whereas the shoreline shows general stability across the investigated period, apart from the mild retreat coupled with bar generation in December 2017.

An analysis of inter-annual and seasonal trends for morphological features in *Terracina* (Fig. 9) confirms a global offshore trend for bar *b1*, with a mean multi-yearly migration rate of 0.08 m/day, and a strong seasonal response with offshore migration mean rates up to 0.6 m/day during winter (Table 2). The new inner bar *b3*, visible for only a year in the observational period, shows a mild onshore trend after its emergence and no significant seasonal response. The shoreline is observed to mildly advance in 2017 in conjunction with the general seaward displacement of bar *b1*, only to retreat the following year when the double bar configuration was established (Fig. 9).

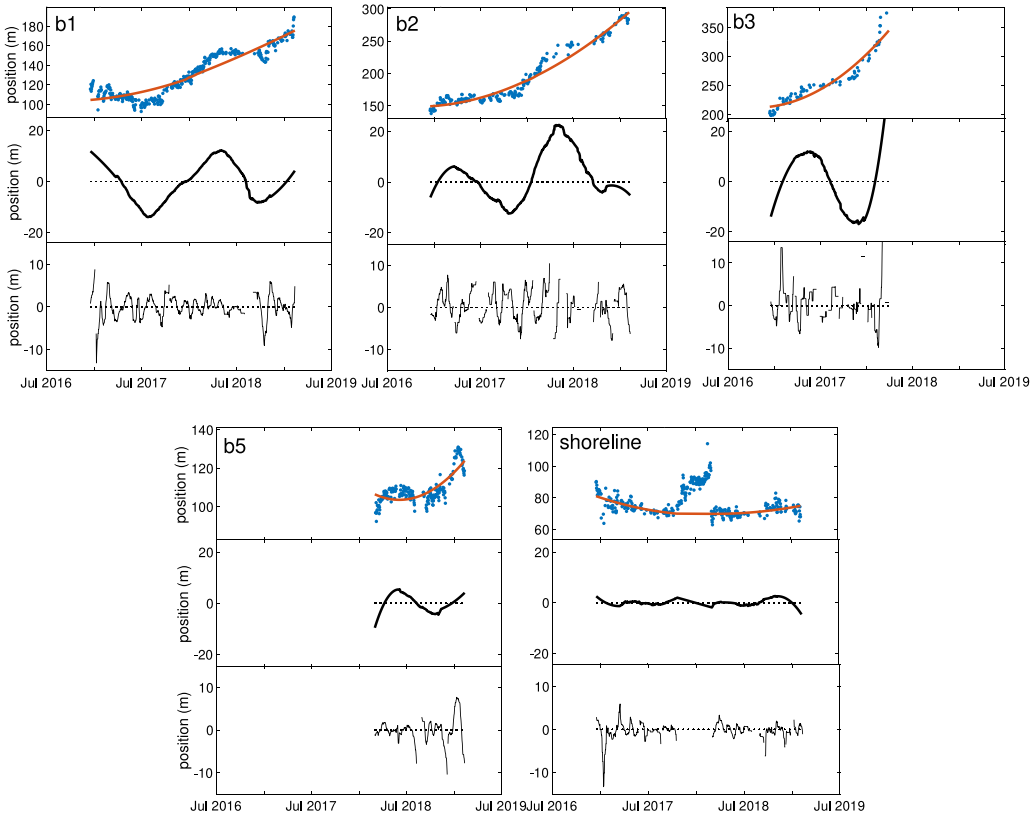

Fig. 7. Annual, seasonal and weekly trends of bar and shoreline migration in *Senigallia*. For each feature (bars and shoreline) the three panels show, from top to bottom: (i) the along-shore averaged cross-shore position (blue dots) and the annual trend (orange line); (ii) the seasonal trends with respect to the annual trend (positive values mean seaward positions and negative values mean landward positions with respect to the annual trend, respectively); (iii) the weekly displacements. Note that a segment of the shoreline location time series corresponding to the generation of the newborn bar *b5* has been removed prior to the trends assessment.

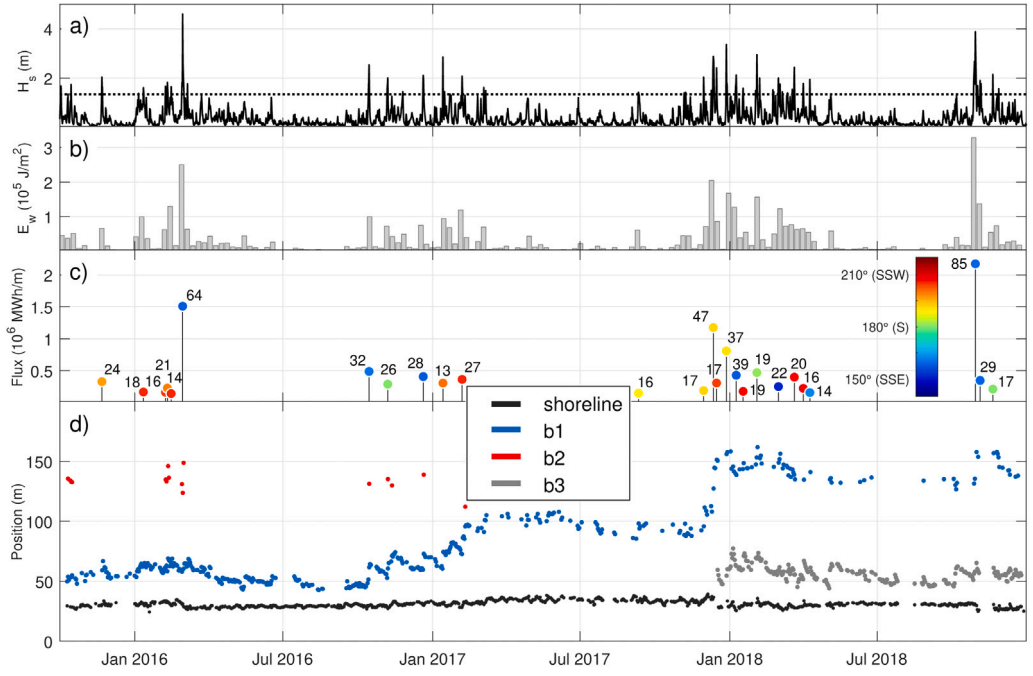

Fig. 8. Wave climate and bar configuration in *Terracina* (October 2015–December 2018). (a) Modelled offshore significant wave height (solid line) and storm threshold (dashed line). (b) Cumulated weekly wave energy. (c) Characterization of classified storms. Stems length represents the energy flux. Numbers represent storm duration (in hours). Marker colours indicate the peak storm wave direction (°N). (d) Cross-shore, alongshore-averaged bar and shoreline position.

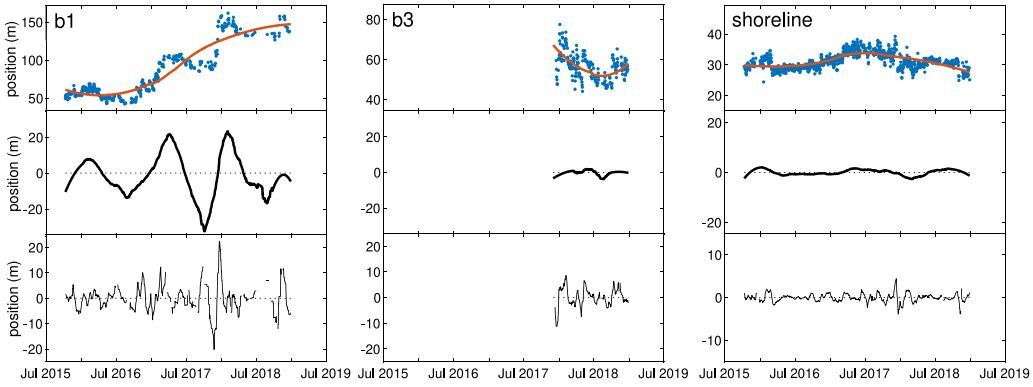

Fig. 9. Annual, seasonal and weekly trends of bar and shoreline migration in *Terracina*. For each feature (bars and shoreline) the three panels show, from top to bottom: (i) the along-shore averaged cross-shore position (blue dots) and the annual trend (orange line); (ii) the seasonal trends with respect to the annual trend (positive values mean seaward positions and negative values mean landward positions with respect to the annual trend); (iii) the weekly displacements.

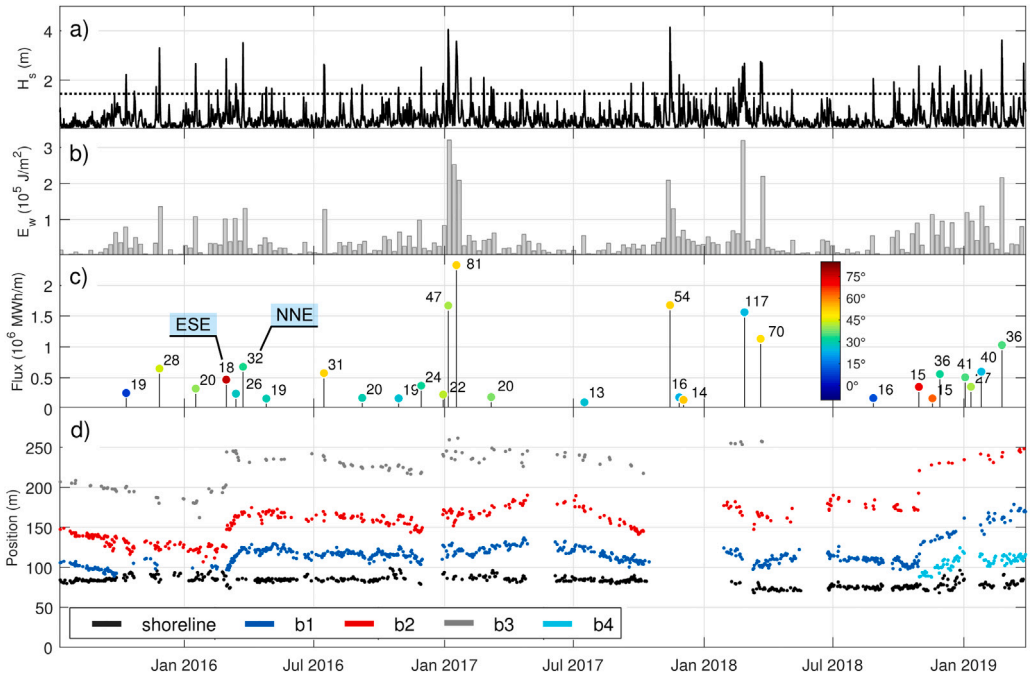

Fig. 10. Wave climate and bar configuration in *Senigallia Estuary* (July 2015–March 2019). (a) Modelled offshore significant wave height (solid line) and storm threshold (dashed line). (b) Cumulated weekly wave energy. (c) Characterization of classified storms. Stems length represents the energy flux. Numbers represent storm duration (in hours). Marker colours indicate the peak storm wave direction (°N). The two storms used for the comparison in Fig. 11 are highlighted with light blue labels. (d) Cross-shore, alongshore-averaged bar position. (For interpretation of the references to colour in this figure legend, the reader is referred to the web version of this article.)

Table 2
Mean inter-annual and seasonal migration rates for the morphological features in *Terracina* shown in Fig. 9. Positive (negative) values indicate offshore (onshore) migration.

Feature	Mean interannual m/day	Seasonal (summer) m/day	Seasonal (winter) m/day
b1 (inner–outer)	0.08	−0.1 – 0	0.1 – 0.6
b3 (inner)	−0.02	−0.06 – 0	−0.05 – 0.05
Shoreline	−0.002	–	–

3.3. Senigallia Estuary

The concrete jetty at the Misa river mouth (Fig. 1c and f) offers a partial shelter from Bora storms (NNE) and generates large lee side vortices when interacting with particularly intense wave from northern directions, but leaves the coast exposed to Scirocco storms (ESE). The jetty is also likely to interact with and reflect littoral currents and waves coming from southern quadrants. This configuration can be exploited to explore to what extent bar migration processes are influenced by the presence of nearby structures in this coastal environment.

Wave climate and bar parameters for *Senigallia Estuary* (July 2015–March 2019) are illustrated in Fig. 10. The submerged beach is here characterized by three sandbars (Fig. 10d). As observed for *Senigallia* (Section 3.1), the coast near the river jetty shows a poor reactivity to single storm events and its morphological response is rather linked to global wave regime, with sometimes sensible onshore migration in summer climate and seaward motion under winter waves.

Notable exceptions to this pattern are two short-lived SSE storms occurred in February 2016 (18 h) and October 2018 (15 h; stems with red markers in Fig. 10c). Both storms managed to strongly move the alongshore-averaged bar position seaward by as much as 50 m for outer bars and 30–40 m for inner bars. The almost-instantaneous migrations of the outer bars left the inner bars and coastline exposed to the action of sustained wave climate in the following months. As a result, the inner bar *b1* gradually moved offshore at a rate of around 1.2 m/day in March

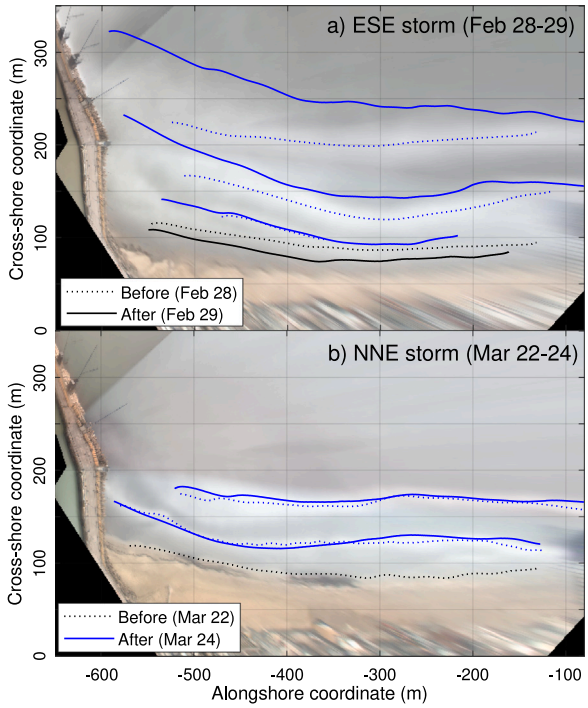

Fig. 11. Remotely sensed sandbar and shoreline positions at *Senigallia Estuary* before and after (a) the February 28–29, 2016 storm (ESE), and (b) the March 22–24, 2016 storm (NNE). Dashed and solid lines mark bars position before and after the storm event, respectively. Bars locations are superimposed to timex images captured by the SGS station at the beginning of each storm. Blue lines represent bars; black lines represent the shoreline. (For interpretation of the references to colour in this figure legend, the reader is referred to the web version of this article.)

2016, and a new inner bar (*b4*) emerged in November 2018 (Fig. 10d). Storms from northern quadrants are not able to significantly modify the cross-shore bar position, although some local changes on a time scale of days can be observed (e.g., see the movements of bars *b1*, *b2*, and *b3* in response to the 81-hour storm in January 2017, Fig. 10c). The surf zone width is narrower than in *Senigallia* and bars tend to be seldomly visible in timex images even at about 150 m from the shoreline (see bar *b3* in February–March 2018; Fig. 10d).

Fig. 11a shows bar location before (dashed lines) and after (solid lines) the 18-hour SSE storm event in February 2016. Bar crest locations before and after a typical NNE storm of comparable intensity (March 22–24, 2016) are also shown for comparison in Fig. 11b. Both storms are evidenced with light blue labels in Fig. 10. The x– and y–axes in Fig. 11 represent, respectively, the alongshore and cross-shore distance with respect to a local reference frame with the origin of the x–axis located near the Rotonda (right side of the panels) and negative x–coordinates directed towards the estuary jetty (left side of the panels). Fig. 11a reveals that the bars experienced a strong offshore migration that is more pronounced for the portion closest to the jetty. The outer bar exhibits as much as 80–100 m of offshore displacement following the storm event. Overall, the migration pattern can be seen as a net rotation around a centre located near the Rotonda pier.

Inter-annual and seasonal trends in Fig. 12 feature strong seasonal response for all bars except for the newborn bar *b4* and the shoreline, while the inter-annual migration is less pronounced than in *Senigallia*. This is reflected by the smaller mean inter-annual and generally larger summer migration rates (in absolute value; Table 3) with respect to those at *Senigallia*. Absolute values of winter migration rates are instead comparable between the two sites. The shoreline is generally unresponsive to seasonal regimes, but presents a retreat of some 10 m after the winter season 2017–2018. Unfortunately, due to the lack of video observations between October 2017 and January 2018 (see the gap in Fig. 10d) it is unclear whether such retreat is caused by single storm action (e.g., by the energetic 54-hour storm in October 2017; 10d) or by globally intense winter climate.

Table 3
Mean inter-annual and seasonal migration rates for the morphological features in *Senigallia Estuary* shown in Fig. 12. Positive (negative) values indicate offshore (onshore) migration. Rates for bar *b4* were not computed, since the limited data available hindered the evaluation of meaningful interannual or seasonal migration rates.

Feature	Mean interannual m/day	Seasonal (summer) m/day	Seasonal (winter) m/day
b1 (inner)	0.05	−0.2 – 0	0 – 0.4
b2 (middle–outer)	0.07	−0.25 – 0.15	−0.2 – 0.5
b3 (outer)	0.06	−0.2 – 0	−0.4 – 0.45
Shoreline	−0.006	–	−0.05 – 0

3.4. Effect of wave height and directionality on bar migration patterns

Fig. 13 presents scatter plots of bar displacement rates at the three sites, as a function of wave height and direction at classified storm peaks. Bar displacement rates are computed by dividing the estimated bar displacement across a single storm event (evaluated on the sum of inter-annual, seasonal, and residual components of the time series of cross-shore feature location; see also Section 2.3) by the storm duration in days. The size of each marker is proportional to the storm-level migration rate experienced by the specific bar when exposed to that storm. Each marker, therefore, expresses the impact that a storm exerts over a specific feature of the coastline, considering its maximum wave height and directionality.

Fig. 13a shows that the highest storm-level responses for bars in *Senigallia* are given by the outer bar *b3* in response to storms with relatively low peak incidence (± 10° with respect to shore normal), but no sign of sensitivity to waves from a particular direction. In *Senigallia Estuary* (Fig. 13b) the presence of the river jetty leaves the coast susceptible to Scirocco storms and the greatest migration rates occur with highly oblique storms (+30°–+40°) and moderate wave energy H_s < 3 m. It is noted that the same storm event generates different responses in terms of sheer bar displacement rates, and the sandbar(s) that is (are) influenced the most by the storm can also be different at the two Adriatic sites. As an example, see the storm event with peak wave incidence +33° and H_s = 2.55 m, ensuing a moderate migration rate mainly on the inner bar *b1* in *Senigallia* (Fig. 13a), while causing high migration rates at both the inner and middle bars *b1* and *b2* in *Senigallia Estuary* (Fig. 13b). In *Terracina* (Fig. 13c) there is a larger number of high migration rate events than for the Adriatic sites, and they are generally seaward-directed (mostly black markers). In particular, the highest rates are exhibited by bar *b1* in response to storms with peak incidence between +10° and +35° , and peak wave height between 1.5 and 3 m. Inner bar *b3*, sheltered by the outer bar *b1*, presents much less variation in comparison.

3.5. Inter-site comparison of storm-induced bar displacements

Fig. 14 displays scatter plots where the energy fluxes of classified storms is plotted against the displacements of each sandbar for the three investigated beaches, to inspect possible relations between storm intensity and morphology. For the sake of inter-site comparison, energy fluxes F and bar displacements Δx_b are made dimensionless as follows:

$$\tilde{F} = F \frac{\beta_0 \sqrt{g d_0}}{\rho g^2 d_0^3}, \tag{7}$$

$$\Delta \tilde{x}_b = \Delta x_b \frac{\beta_0}{d_0}, \tag{8}$$

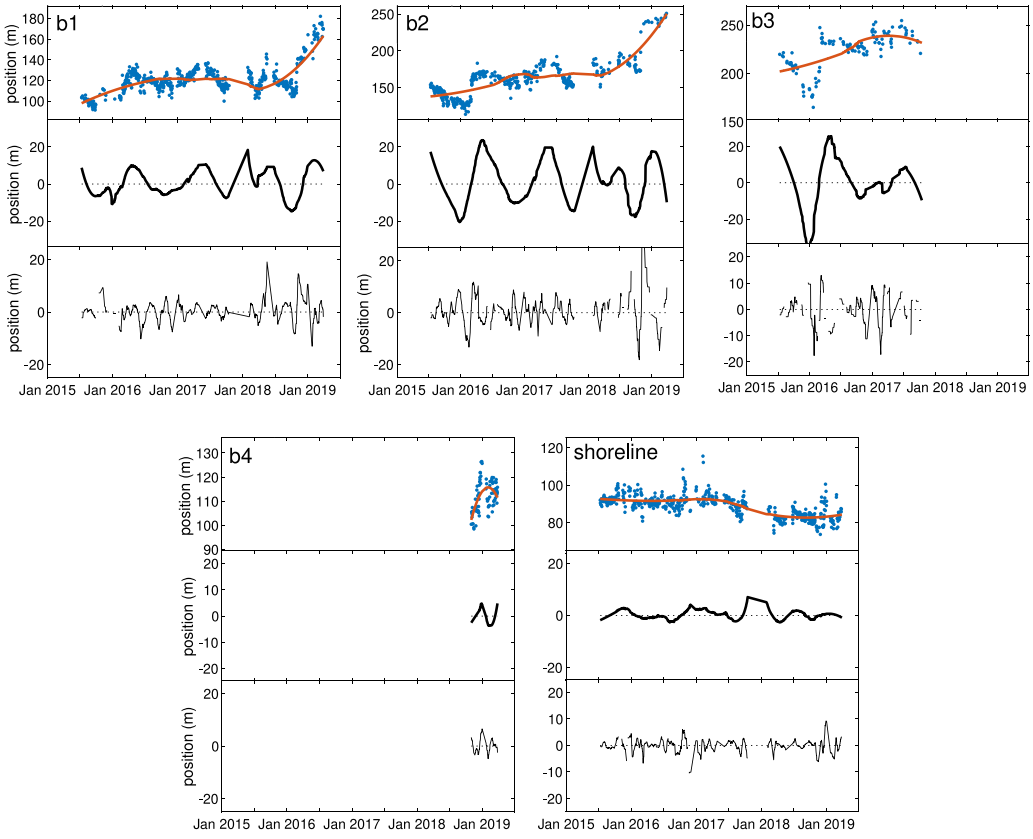

Fig. 12. Annual, seasonal and weekly trends of bar and shoreline migration in *Senigallia Estuary*. For each feature (bars and shoreline) the three panels show, from top to bottom: (i) the along-shore averaged cross-shore position (blue dots) and the annual trend (orange line); (ii) the seasonal trends with respect to the annual trend (positive values mean seaward positions and negative values mean landward positions with respect to the annual trend, respectively); (iii) the weekly displacements.

where d_0 is the water depth at the points where the wave climate data are obtained (d_0 = 10.5 m for *Senigallia* and *Senigallia Estuary*; d_0 = 13.5 m for *Terracina*) and β_0 is the representative seabed slope at the same points (β_0 = 0.005 for *Senigallia* and *Senigallia Estuary*; β_0 = 0.02 for *Terracina*). The scaling has been performed in order to make the comparison independent from site-specific quantities, such as the bottom slope and the water depth at the point of wave data extraction, so that the relevant features of bar displacement could be compared across all beaches. Cross-shore and longshore components of energy fluxes are obtained as per Eqs. (2) and (3), with θ_m evaluated at storm peak. Only bar displacements larger than ± 5 m are shown. For sandbars data for which a correlation could be inferred, the best fit line is also plotted. The fit lines have been forced to start from the origin.

Both the unbounded beaches of *Senigallia* (Fig. 14a) and *Terracina* (Fig. 14c) have a general positive correlation between total storm intensity and bar displacements, due to the beaches presenting mainly offshore-directed migration events across single storms. However, the magnitudes of bar displacements are notably different between the two sites. For storms with the same intensity ($\tilde{F}$ = 0–1), bar motions at *Terracina* are often twice or more intense than those at *Senigallia*, this difference being thus ascribed to morphological differences between the two beaches. On the other hand, at the bounded beach of *Senigallia Estuary* no such correlation is observed, due to occurrences of both onshore- and offshore-directed motions that are apparently unrelated to general storm intensity (Fig. 14b). Only for bar *b2* a slightly positive relation could be found (dashed line in Fig. 14b). However, correlations are to be taken as qualitative, since the coefficients of determination r^2 are consistently low (r^2 = 0.05–0.5), due to the large data scatter preventing a meaningful quantitative correlation. The same qualitative correlations (or lack thereof) are retrieved when only the cross-shore flux component is considered ($\tilde{F}_x$; Fig. 14d–f), implying that cross-shore processes are the most dominant in defining bar dynamics at the study beaches.

Interestingly, when the longshore component of storm energy flux is considered ($\tilde{F}_y$; Fig. 14g–i), mild positive correlations arise for *Senigallia Estuary* (Fig. 14h). This is related to an occurrence of mainly positive (offshore) displacements in storms with a positive peak angle of incidence (south-eastern storms; red markers), whereas near-zero or negative (stable or onshore) displacements are observed for storms with negative angle of incidence (northern storms; blue markers). The remarkable similarity in the cross-shore bathymetry between *Senigallia* and *Senigallia Estuary* (Fig. 2) and the general alongshore uniformity of sandbars suggest that the increased correlation to longshore fluxes is due to the presence of the morphological constraint imposed by the jetty, rather than by differences in the seabed morphology. No relevant relations to longshore fluxes are indeed observed at the other two (unbounded) locations (Fig. 14g and i).

4. Discussion

The analysis of bar dynamics proposed in this study has shown various levels of cross-shore mobility for sandbars at all the investigated beaches across the study years, even though in response to remarkably different wave climates and at different time scales. In these microtidal settings, breaking patterns are not critically modulated by tide; therefore, the wave action can be regarded as the main driver of morphological changes.

Seaward bar motions at the Adriatic sites of *Senigallia* and *Senigallia Estuary* appear to be mainly controlled by seasonal oscillations, with relative stability or slight onshore motion with mild summer waves and regular offshore motion during winter (Figs. 5 and 10). Storm-level

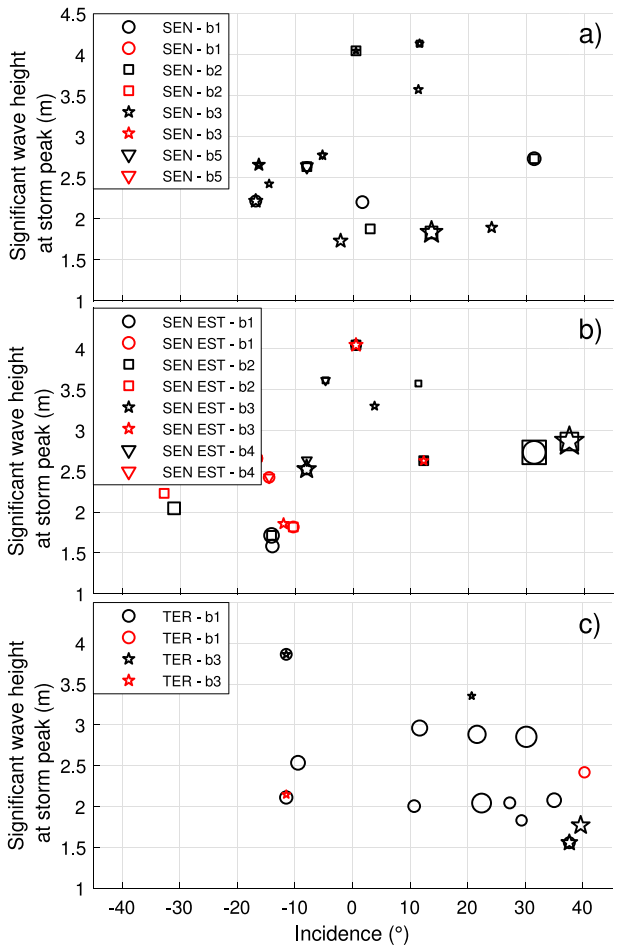

Fig. 13. Scatter plots of bar migration events during classified storm, as a function of the offshore wave climate (H_s) and wave incidence at storm peaks, in (a) *Senigallia*, (b) *Senigallia Estuary*, and (c) *Terracina*. The dimension of each marker is proportional to the displacement rate observed by the specific bar. Black markers represent offshore migration; red markers represent onshore migration. (For interpretation of the references to colour in this figure legend, the reader is referred to the web version of this article.)

response here is generally weak. On the other hand, bars in *Terracina*, while still showing different responses in relation to wave seasonality, are more sensible to single storm events and their net seaward displacement should be seen as the product of storm sequencing rather than the overall intensification of wave climate in winter months (Fig. 8).

At a storm-level scale, the overall bar dynamics appears not to be dominantly controlled by the offshore wave height. Generally, the storms with the highest peak H_s are not those which generate the largest bar displacements (Fig. 13). Bar motions are rather more relatable to energy-based parameters like the wave energy flux, and particularly its cross-shore component (top and middle rows in Fig. 14), suggesting that wave power normal to the shoreline is the main forcing of morphology changes at the investigated beaches. Although bar dynamics do not show significant correlation with the offshore H_s, the relative wave height over the submerged bars is of importance in defining the local, event-scale behaviour of the bar system (see Section 4.2).

4.1. NOM patterns and dependence on morphological factors

As a result of generalized offshore trends, all the studied sites show the establishment of at least one well-defined NOM cycle (Ruessink and Kroon, 1994) with a more or less gradual migration of bars outside of the bar zone, their decay, and subsequent generation of new inner bars triggered by energetic storm events or clusters. The recurrence of such cycle, consistent with observations of NOM patterns along other microtidal Mediterranean coasts (Guillén and Palanques, 1993; Aleman et al., 2013) as well as along multi-barred beaches in mesotidal environments (Ruessink and Kroon, 1994; Wijnberg and Terwindt, 1995; Shand and Bailey, 1999), further reinforces the idea that, although single bars may indeed tend towards an equilibrium point dependent on local wave climate, the overall bar system may never reach a stable equilibrium in the long term (Plant et al., 2001; Swart, 1974; Atkinson, 2018).

The overall similarity in wave conditions (offshore average wave parameters and seasonality) and geological properties (mean sand size) suggests that the observed differences in NOM characteristics across Adriatic and Tyrrhenian sites are reasonably more related to differences in seabed morphology and geometry of the bar system, and consequently to the way wave-generated forcings are distributed across and interact with the beach profile. The mildly sloping beach of *Senigallia* presents a uniform, inter-annual offshore trend superimposed with increased offshore rates during winter months (Parlagreco et al., 2019). This pattern closely resembles that of bars along the coast of Egmond, The Netherlands (Pape et al., 2010), with which shares similar mean surf zone slopes (around 0.01). Conversely, the quick response times to storm events and following recovers in mild climate observed in *Terracina* are similar to those experienced by bars at the Gold Coast, Australia (Pape et al., 2010) (mean surf zone slope of about 0.015–0.02). Similarities between locations can also be described by means of the Iribarren number:

$$\mathrm{Ir} = \frac{\beta}{\sqrt{H/L_0}}, \tag{9}$$

where $L_0 = \frac{gT^2}{2\pi}$ is the deep water wave length. Assuming yearly mean wave climate data for *Senigallia* and Egmond yields closely comparable Iribarren numbers. The same thing happens adopting yearly maximum wave data for *Terracina* and the Gold Coast (Table 4).

Other morphological factors, like the bars size and the surf zone width, are supposed to have a role on the time scale at which NOM events occur (Ruessink et al., 2009; Tătui et al., 2016). Coastal systems with large bars and wider breaking zones may experience inter-annual systematic NOM behaviour, whereas limited-size bars may exhibit NOM patterns at time scales of single storm events or clusters, or seasonally. A wider breaking zone in *Senigallia* (around 300 m, from the outermost to the innermost bars; Fig. 2) suggests a gradual energy dissipation across the surf zone. This may hinder the development of strong undertow processes, especially over the inner bars, and thus limit the storm-scale response of those bars in favour of seasonal–interannual trends. On the other hand, in *Terracina* a steeper lower shoreface and a reduced number of bars (Fig. 2) may lead to focussing of wave dissipation over the narrow bars and development of strong undertow, which may ultimately explain the sharp response of submerged bars to storm events. In both cases, surf zone processes, such as offshore migration in response to strong breaking and mild onshore motion due to surf bores, appear to be dominant (although with different magnitudes) as suggested by Price and Ruessink (2008) for barred microtidal beaches.

Also the seaward limit of the active bar region, where the sand bars ultimately decay, appears to be here controlled by morphological-related parameters, more than by wave forcing. The most offshore evidences of bars are detected as far as 250–300 m from the shoreline in *Senigallia* (Fig. 5), but only at around 130 m in *Terracina* (Fig. 8), in spite of the globally similar wave climate typical of the Mediterranean sea. Di Leonardo and Ruggiero (2015), discussing an extensive bathymetric data set for the mesotidal US Pacific Northwest, observed a similar result, with steeper parts of the coast presenting bars closer to the shoreline than mildly sloping parts. The strong reduction of the hydrodynamic forcing over bars, due to the sandy features gradually moving towards higher depths and decreasing their interaction with waves, is indeed suggested as one of the most important bar-depleting conditions (Wijnberg, 1997); this finding is further reinforced by experimental evidence (see, e.g., Atkinson, 2018).

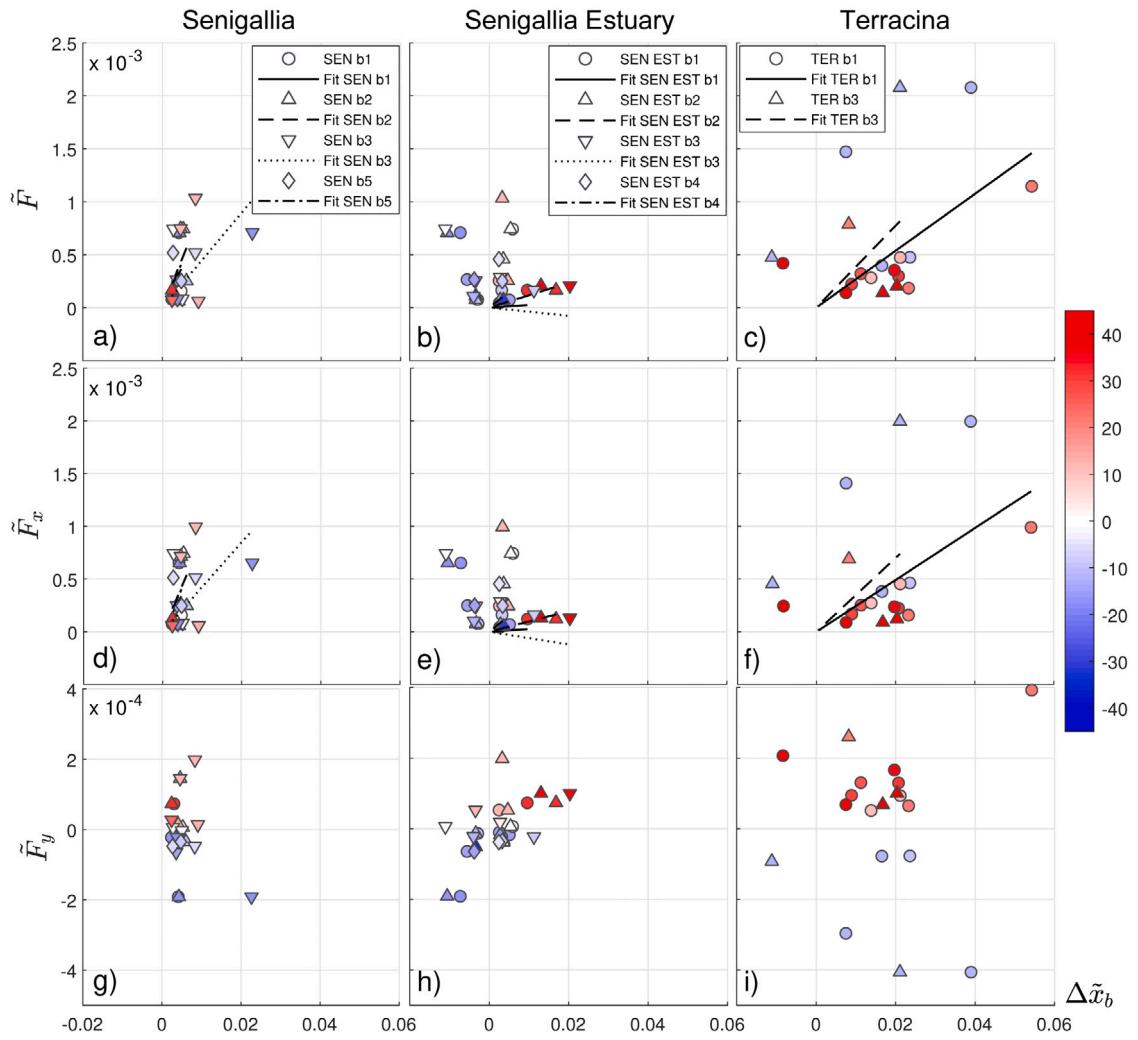

Fig. 14. Scatter plots of bar displacements against (a, b, c) total, (d, e, f) cross-shore components, and (g, h, i) longshore components of storm energy fluxes, for *Senigallia* (left column), *Senigallia Estuary* (middle column), and *Terracina* (right column). Marker colours represents storm peak wave incidence. Positive (red) and negative (blue) incidence angles represent clockwise and anti-clockwise direction with respect to shore normal, respectively. Positive and negative displacements indicate offshore and onshore motions, respectively. Positive cross-shore energy fluxes are directed onshore. Positive longshore fluxes are directed leftward. Best fitting lines are plotted in the top and middle rows of panels. Note the different scale for longshore energy fluxes in panels (g, h, i). (For interpretation of the references to colour in this figure legend, the reader is referred to the web version of this article.)

Table 4
Estimated values of the Iribarren number for the beaches of *Senigallia* and *Terracina* and comparison with values for the beaches of Egmond and Gold Coast.

Site	Reference	H_m, H_{max}	T_m, T_{max}	β	Ir
Senigallia		0.44[a]	4.1[a]	0.009	0.07
Egmond	Price and Ruessink (2008) and Pape et al. (2010)	1.2[a]	4.5[a]	0.01	0.06
Terracina		4.6[b]	12[b]	0.018	0.126
Gold Coast	Turner et al. (2004) and Pape et al. (2010)	5.0[b]	14[b]	0.017	0.13

[a]Mean values.
[b]Maximum values.

4.2. Effect of adjacent structures and wave directionality at a bounded beach: Senigallia Estuary

Although the environmental and geographical conditions are the same between the two beaches on the Adriatic side, the presence of a concrete jetty delimiting the northern border of the *Senigallia Estuary* beach (Fig. 1c and f and Fig. 10) has been shown to alter the bar dynamics when compared to the unbounded beach of *Senigallia*. A mostly seasonal response and the overall absence of sharp bar motions due to storm events make the typical behaviour of the bar system of *Senigallia Estuary* somehow similar to that of *Senigallia*, with bars at *Senigallia Estuary* experiencing seasonally-modulated oscillations reminiscent of an OPE-like behaviour (Certain and Barusseau, 2005). However, the reactivity of bars to storms from southern quadrants is enhanced to the point of generating strong bar migration and also an episodic NOM, i.e. related to a single, extreme storm event (Ruessink et al., 2009), as those observed at the beach of *Terracina*. Also the seasonality of bar migration appears to be slightly enhanced by the presence of the jetty, as the onshore migration trends with mild waves are more apparent than in *Senigallia* (Fig. 10) and summer mean migration rates are higher and mostly shoreward (Table 3).

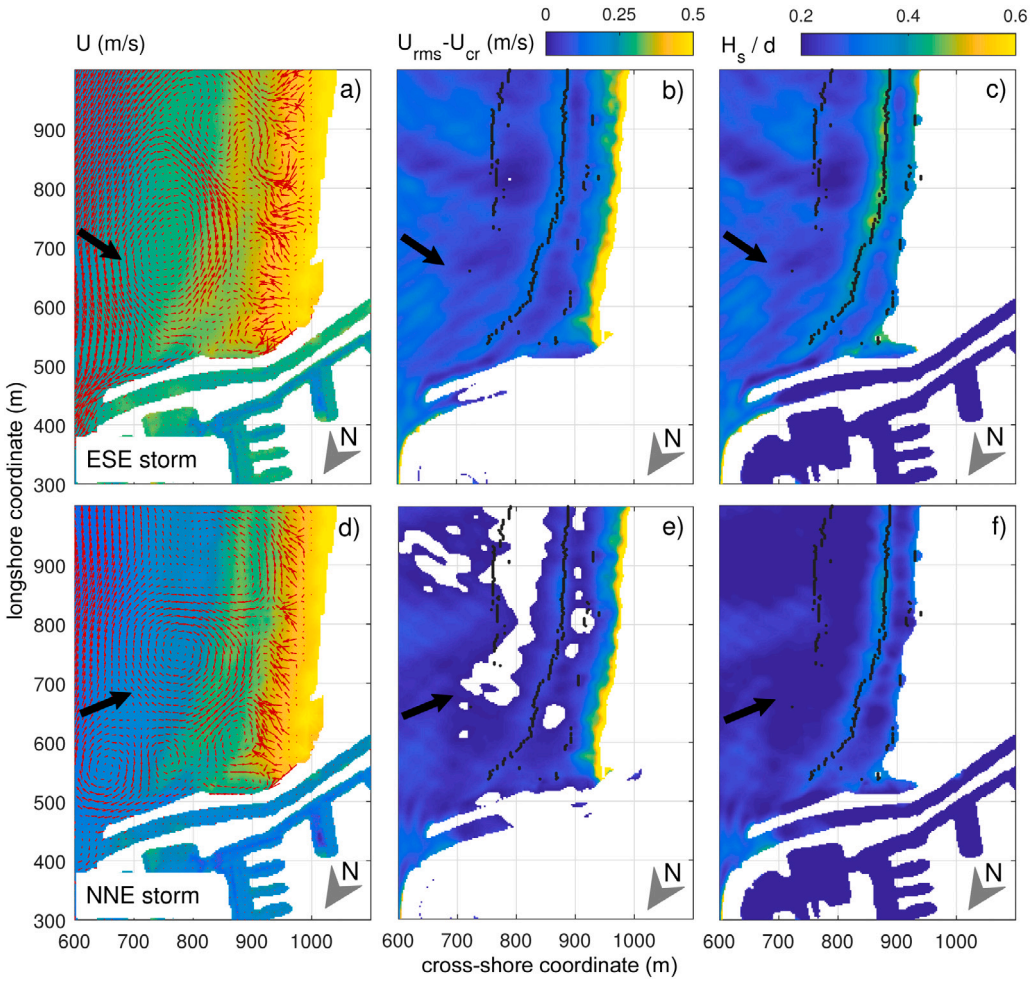

Fig. 15. (a, d) Fields of 30-minute averaged, depth-averaged velocity U, (b, e) difference between root-mean-square bottom orbital velocity due to waves and critical value for sediment motion $U_{rms} - U_{cr}$, and (c, f) ratio of significant wave height to water depth H_s/d for the simulated ESE storm (top row) and NNE storm (bottom row), after 6 h of simulated time. Bar crests in the DTM are evidenced with black dots. Black arrows show the direction of wave attack.

The altered bar dynamics at *Senigallia Estuary* is also reflected by the displacement of bar lines during a typical ESE storm (Fig. 11a), which can be seen as a bar rotation often studied in the context of embayed beaches (van de Lageweg et al., 2013; Blossier et al., 2016). Bar rotation is linked to two possible mechanisms: a pivotal rotation mechanism associated with longitudinal variations of wave energy due to wave shadowing and sheltering, and a migration-driven mechanism determined by differential bar migration rates in the alongshore direction (Blossier et al., 2016). At *Senigallia Estuary* the migration-driven mechanism seems dominant, as the Rotonda pier (at the right ends of the panels in Fig. 11) offers little to no sheltering from ESE storms due to its limited length and high permeability. On the other hand, the bar rotation can be clearly seen as a differential bar migration, which is larger for the portions closer to the river jetty (Fig. 11a). This behaviour is likely induced by alongshore differences in the magnitude of cross-shore processes due to the presence of the jetty, as also hypothesized by van de Lageweg et al. (2013).

Numerical explorations of the hydrodynamics at *Senigallia Estuary* with the use of FUNWAVE show that differences arise in circulation patterns and sediment stirring velocities between characteristic storms from the two main directions. 30-minute-averaged fields of depth-averaged velocity U (Fig. 15a and d) reveal that the representative ESE storm is characterized by the development of a sustained southward-directed longshore current over the bar, part of a major anti-clockwise circulation cell that joins a strong alongshore current further offshore (Fig. 15a). The NNE storm, on the other hand, induces smaller fragmented coherent structures. The model still predicts a longshore flow, this time towards the river jetty (Fig. 15d). Potential for sediment motion, evaluated by means of the difference between U_{rms} and U_{cr}, is predicted to occur above the bar for both storms (Fig. 15b and e), but the magnitude of such difference is greater for the ESE storm over all the nearshore region, thus suggesting a greater influence of ESE storms on potential wave-related sediment transport.

The occurrence of seaward or shoreward bar migration can be also linked to the relative wave height over bars. Ruessink and Terwindt (2000) suggested that values of H_s/d larger than 0.6 may lead to a dominance of offshore sediment transport and thus seaward migration, whereas values smaller that 0.3 to a tendency for onshore migration. The ratio H_s/d is also connected to the development of the undertow current in the formulation of Abreu et al. (2012), as well as to the potential for erosion/accretion around underwater structures in Postacchini et al. (2016). Estimates of relative wave height for both storms (Fig. 15c and f) indeed predict average values of H_s/d up to about 0.5–0.55 across the middle bar for the ESE storm (Fig. 15c), while the values are smaller (up to about 0.35–0.4) for the NNE storm (Fig. 15f). This suggests a relevance of offshore-directed sediment processes at the top of bars for storms from southern quadrants.

4.3. Future perspectives

In the view of discussing common traits and similarities across a number of beaches in a compact way, only the alongshore-averaged bar position has been considered as a morphological indicator in this

work. Nonetheless, a more comprehensive discussion of sandbar features would greatly benefit from considering also alongshore bar non-uniformities, i.e. crescentic bar structures (Bowen and Inman, 1971), which are not uncommon features along Mediterranean coasts, especially with low-to-moderate wave climate (Parlagreco et al., 2011; Armaroli et al., 2007; Armaroli and Ciavola, 2011). Moreover, some studies highlighted the key role of beach morphology antecedent to storms or storm sequences in defining beach dynamics during extreme events (Morales-Márquez et al., 2018). Due to the lack of extensive bathymetric survey data in both time and space for the investigated beaches, these aspects have not been considered in this study, but they might be tackled in future research.

5. Conclusions

We have presented novel video-based observations of submerged bars at three microtidal environments typical of Italian coasts, and attempted a correlation of bar dynamics to the wave climate and the presence of rigid coastal structures. This study adds to the still scarce literature devoted to the characterization of bar dynamics in the Mediterranean sea and in microtidal contexts in general.

We have given first evidence, to the best of the authors' knowledge, that the NOM model for bar migration, firstly defined and frequently observed in macrotidal and highly energetic beaches, applies also to bar systems in the Adriatic sea. Net offshore migration of bars towards higher depths (about 300 m from the shoreline) and generation of a new inner bar have been observed in the unbounded beach of *Senigallia*, in spite of the generally modest wave energy. Bar motions here are mainly dominated by seasonal modulations of wave climate. No significant response to single storms or sensitivity to storm energy or wave direction has been assessed. NOM-like patterns also occurred at the unbounded beach of *Terracina*, but unlike at *Senigallia*, bars exhibit a strong response to single storms and storm sequences, with event-related displacements reaching up to 50 m. Due to the orientation of the coast, the highest migration rates have been observed in response to storms with a high incidence angle, although not those with the highest significant wave height.

Our study suggests that the mean beach slope and global bar morphology are key controlling factors in determining the overall features of bar migration, with lower slopes promoting more uniform, multi-annual migration trends, and steeper slopes and bars favouring storm-event response thanks to shoaling and more pronounced wave breaking.

A concrete jetty near the beach of *Senigallia Estuary* allowed us to inspect the effects of artificial boundaries at a slightly embayed beach subjected to the same wave climate of *Senigallia*. Bars here exhibited a singular combination of OPE-like oscillations modulated by seasonal wave climate, superimposed with occasional, strong NOM events triggered by ESE storms and intensified by the presence of the jetty. Numerical simulations suggest that storms from ESE may generate sustained longshore currents and circulation patterns over bars, which in conjunction with more intense bottom orbital velocities and higher relative wave heights promote a stronger offshore-directed sediment transport, and subsequently bar seaward migration in comparison with NNE storms.

CRediT authorship contribution statement

Lorenzo Melito: Conceptualization, Methodology, Software, Formal analysis, Investigation, Data curation, Writing - original draft, Visualization. **Luca Parlagreco:** Conceptualization, Methodology, Software, Formal analysis, Resources, Data curation, Writing - review & editing, Supervision, Funding acquisition. **Eleonora Perugini:** Conceptualization, Software, Formal analysis, Resources, Data curation, Writing - review & editing. **Matteo Postacchini:** Conceptualization, Methodology, Formal analysis, Writing - review & editing, Visualization, Supervision. **Saverio Devoti:** Software, Resources, Data curation, Funding acquisition. **Luciano Soldini:** Software, Data curation, Writing - review & editing, Supervision. **Gianluca Zitti:** Conceptualization, Methodology, Writing - review & editing. **Luca Liberti:** Software, Resources. **Maurizio Brocchini:** Conceptualization, Writing - review & editing, Supervision, Funding acquisition.

Declaration of competing interest

The authors declare that they have no known competing financial interests or personal relationships that could have appeared to influence the work reported in this paper.

Acknowledgements

This study is funded by Circeo National Park, Gargano National Park and the "Torre del Cerrano" Marine Protected Area within the National Biodiversity Strategy promoted by the Ministero dell'Ambiente e della Tutela del Territorio e del Mare (MATTM), Italy (GAB0024444). The financial support from the Office of Naval Research Global (UK) MORSE Project (Research Grant Number N62909-17-1-2148) and the MIUR PRIN 2017 Project, Italy "FUNdamentals of BREAKing wave-induced boundary dynamics – FUNBREAK" (Grant Number 20172B7MY9) is gratefully acknowledged. The authors would like to thank the two anonymous reviewers whose suggestions improved the original manuscript.

References

Aagaard, T., Davidson-Arnott, R., Greenwood, B., Nielsen, J., 2004. Sediment supply from shoreface to dunes: linking sediment transport measurements and long-term morphological evolution. Geomorphology 60 (1–2), 205–224. http://dx.doi.org/10.1016/j.geomorph.2003.08.002.

Aagaard, T., Nielsen, J., Greenwood, B., 1998. Suspended sediment transport and nearshore bar formation on a shallow intermediate-state beach. Mar. Geol. 148 (3–4), 203–225. http://dx.doi.org/10.1016/s0025-3227(98)00012-7.

Abreu, T., Sancho, F., Silva, P.A., 2012. Influence of non-linear waves and undertow in sandbar development. Coast. Eng. Proc. 1 (33), 55. http://dx.doi.org/10.9753/icce.v33.sediment.55.

Aleman, N., Robin, N., Certain, R., Barusseau, J.-P., Gervais, M., 2013. Net offshore bar migration variability at a regional scale: Inter-site comparison (Languedoc-Roussillon, France). J. Coast. Res. 165, 1715–1720. http://dx.doi.org/10.2112/si65-290.1.

Angnuureng, D.B., Almar, R., Senechal, N., Castelle, B., Addo, K.A., Marieu, V., Ranasinghe, R., 2017. Shoreline resilience to individual storms and storm clusters on a meso-macrotidal barred beach. Geomorphology 290, 265–276. http://dx.doi.org/10.1016/j.geomorph.2017.04.007.

Armaroli, C., Ciavola, P., 2011. Dynamics of a nearshore bar system in the northern Adriatic: A video-based morphological classification. Geomorphology 126 (1–2), 201–216. http://dx.doi.org/10.1016/j.geomorph.2010.11.004.

Armaroli, C., Ciavola, P., Caleffi, S., Gardelli, M., 2007. Morphodynamics of nearshore rhythmic forms: An energy-based classification. In: Coastal Engineering 2006. World Scientific Publishing Company, pp. 4009–4021. http://dx.doi.org/10.1142/9789812709554_0337.

Atkinson, A.L., 2018. Laboratory Beach Profile Dynamics and Responses to Changing Water Levels with and without Nourishment (ph.d. thesis). Civil Engineering, http://dx.doi.org/10.14264/uql.2018.739.

Birkemeier, W.A., 1985. Time scales of nearshore profile changes. In: Coastal Engineering 1984. American Society of Civil Engineers, pp. 1507–1521. http://dx.doi.org/10.1061/9780872624382.103.

Blossier, B., Bryan, K.R., Daly, C.J., Winter, C., 2016. Nearshore sandbar rotation at single-barred embayed beaches. J. Geophys. Res.: Oceans 121 (4), 2286–2313.

Boccotti, P., 2000. Wave Mechanics for Ocean Engineering, Vol. 64. Elsevier.

Bowen, A.J., Inman, D.L., 1971. Edge waves and crescentic bars. J. Geophys. Res. 76 (36), 8662–8671. http://dx.doi.org/10.1029/jc076i036p08662.

Brocchini, M., 2019. Wave-forced dynamics in the nearshore river mouths, and swash zones. Earth Surf. Process. Landf. 45 (1), 75–95. http://dx.doi.org/10.1002/esp.4699.

Brocchini, M., Calantoni, J., Postacchini, M., Sheremet, A., Staples, T., Smith, J., Reed, A.H., Braithwaite, E.F., Lorenzoni, C., Russo, A., Corvaro, S., Mancinelli, A., Soldini, L., 2017. Comparison between the wintertime and summertime dynamics of the Misa River estuary. Mar. Geol. 385, 27–40. http://dx.doi.org/10.1016/j.margeo.2016.12.005.

Certain, R., Barusseau, J.-P., 2005. Conceptual modelling of sand bars morphodynamics for a microtidal beach (Sète, France). Bull. Soc. Geol. France 176 (4), 343–354. http://dx.doi.org/10.2113/176.4.343.

de Swart, R.L., Ribas, F., Calvete, D., Kroon, A., Orfila, A., 2020. Optimal estimations of directional wave conditions for nearshore field studies. Cont. Shelf Res. 196, 104071. http://dx.doi.org/10.1016/j.csr.2020.104071.

Di Leonardo, D., Ruggiero, P., 2015. Regional scale sandbar variability: Observations from the U.S. Pacific Northwest. Cont. Shelf Res. 95, 74–88. http://dx.doi.org/10.1016/j.csr.2014.12.012.

Evangelista, S., Full, W.E., La Monica, G.B., Nelson, D., 2004. Aspects of littoral dynamics along the Circeo-Terracina coastal area (Lazio-Italia Centrale). Geol. Romana 37, 127–130.

Fernández-Mora, A., Calvete, D., Falqués, A., de Swart, H.E., 2015. Onshore sandbar migration in the surf zone: New insights into the wave-induced sediment transport mechanisms. Geophys. Res. Lett. 42 (8), 2869–2877. http://dx.doi.org/10.1002/2014gl063004.

Gallagher, E.L., Elgar, S., Guza, R.T., 1998. Observations of sand bar evolution on a natural beach. J. Geophys. Res.: Oceans 103 (C2), 3203–3215. http://dx.doi.org/10.1029/97jc02765.

Guillén, J., Palanques, A., 1993. Longshore bar and trough systems in a microtidal, storm-wave dominated coast: The ebro delta (Northwestern Mediterranean). Mar. Geol. 115 (3–4), 239–252. http://dx.doi.org/10.1016/0025-3227(93)90053-x.

Hoefel, F., Elgar, S., 2003. Wave-induced sediment transport and sandbar migration. Science 299 (5614), 1885–1887. http://dx.doi.org/10.1126/science.1081448.

Holman, R., Sallenger, A., Lippmann, T., Haines, J., 1993. The application of video image processing to the study of nearshore processes. Oceanography 6 (3), 78–85. http://dx.doi.org/10.5670/oceanog.1993.02.

Houser, C., Greenwood, B., 2007. Onshore migration of a swash bar during a storm. J. Coast. Res. 231, 1–14. http://dx.doi.org/10.2112/03-0135.1.

Komar, P.D., Miller, M.C., 1973. The threshold of sediment movement under oscillatory water waves. J. Sediment. Res. 43 (4), 1101–1110. http://dx.doi.org/10.1306/74d7290a-2b21-11d7-8648000102c1865d.

Korres, G., Ravdas, M., Zacharioudaki, A., 2019. Mediterranean Sea Waves Hindcast (CMEMS MED-Waves). Copernicus Monitoring Environment Marine Service (CMEMS), http://dx.doi.org/10.25423/CMCC/MEDSEA_HINDCAST_WAV_006_012.

Kuriyama, Y., 2002. Medium-term bar behavior and associated sediment transport at Hasaki, Japan. J. Geophys. Res. 107 (C9), http://dx.doi.org/10.1029/2001jc000899.

Lippmann, T.C., Holman, R.A., 1989. Quantification of sand bar morphology: A video technique based on wave dissipation. J. Geophys. Res. 94 (C1), 995–1011. http://dx.doi.org/10.1029/jc094ic01p00995.

Lippmann, T.C., Holman, R.A., 1990. The spatial and temporal variability of sand bar morphology. J. Geophys. Res. 95 (C7), 11575. http://dx.doi.org/10.1029/jc095ic07p11575.

Lippmann, T.C., Holman, R.A., Hathaway, K.K., 1993. Episodic, nonstationary behavior of a double bar system at Duck, North Carolina, USA, 1986–1991. J. Coast. Res. 49–75.

Masselink, G., 2004. Formation and evolution of multiple intertidal bars on macrotidal beaches: Application of a morphodynamic model. Coast. Eng. 51 (8–9), 713–730. http://dx.doi.org/10.1016/j.coastaleng.2004.07.005.

Morales-Márquez, V., Orfila, A., Simarro, G., Gómez-Pujol, L., Álvarez-Ellacuría, A., Conti, D., Galán, Á., Osorio, A.F., Marcos, M., 2018. Numerical and remote techniques for operational beach management under storm group forcing. Nat. Hazards Earth Syst. Sci. Discuss. 1–25. http://dx.doi.org/10.5194/nhess-2018-173.

Pape, L., Plant, N.G., Ruessink, B.G., 2010. On cross-shore migration and equilibrium states of nearshore sandbars. J. Geophys. Res. 115 (F3), http://dx.doi.org/10.1029/2009jf001501.

Parlagreco, L., Archetti, R., Simeoni, U., Devoti, S., Valentini, A., Silenzi, S., 2011. Video-monitoring of a barred nourished beach (Latium, Central Italy). J. Coast. Res. 110–114.

Parlagreco, L., Melito, L., Devoti, S., Perugini, E., Soldini, L., Zitti, G., Brocchini, M., 2019. Monitoring for coastal resilience: Preliminary data from five Italian sandy beaches. Sensors 19 (8), 1854. http://dx.doi.org/10.3390/s19081854.

Phillips, M.S., Harley, M.D., Turner, I.L., Splinter, K.D., Cox, R.J., 2017. Shoreline recovery on wave-dominated sandy coastlines: The role of sandbar morphodynamics and nearshore wave parameters. Mar. Geol. 385, 146–159. http://dx.doi.org/10.1016/j.margeo.2017.01.005.

Plant, N.G., Freilich, M.H., Holman, R.A., 2001. Role of morphologic feedback in surf zone sandbar response. J. Geophys. Res.: Oceans 106 (C1), 973–989. http://dx.doi.org/10.1029/2000JC900144.

Plant, N.G., Holman, R.A., Freilich, M.H., Birkemeier, W.A., 1999. A simple model for interannual sandbar behavior. J. Geophys. Res.: Oceans 104 (C7), 15755–15776. http://dx.doi.org/10.1029/1999jc900112.

Postacchini, M., Russo, A., Carniel, S., Brocchini, M., 2016. Assessing the hydro-morphodynamic response of a beach protected by detached, impermeable, submerged breakwaters: A numerical approach. J. Coast. Res. 32 (3), 590–602. http://dx.doi.org/10.2112/jcoastres-d-15-00057.1.

Postacchini, M., Soldini, L., Lorenzoni, C., Mancinelli, A., 2017. Medium-term dynamics of a middle Adriatic barred beach. Ocean Sci. 13 (5), 719–734. http://dx.doi.org/10.5194/os-13-719-2017.

Price, T.D., Ruessink, B.G., 2008. Morphodynamic zone variability on a microtidal barred beach. Mar. Geol. 251 (1–2), 98–109. http://dx.doi.org/10.1016/j.margeo.2008.02.008.

Roelvink, J.A., Stive, M.J.F., 1989. Bar-generating cross-shore flow mechanisms on a beach. J. Geophys. Res. 94 (C4), 4785–4800. http://dx.doi.org/10.1029/jc094ic04p04785.

Ruessink, B.G., Kroon, A., 1994. The behaviour of a multiple bar system in the nearshore zone of Terschelling, the Netherlands: 1965–1993. Mar. Geol. 121 (3–4), 187–197. http://dx.doi.org/10.1016/0025-3227(94)90030-2.

Ruessink, B.G., Pape, L., Turner, I.L., 2009. Daily to interannual cross-shore sandbar migration: Observations from a multiple sandbar system. Cont. Shelf Res. 29 (14), 1663–1677. http://dx.doi.org/10.1016/j.csr.2009.05.011.

Ruessink, B.G., Terwindt, J.H.J., 2000. The behaviour of nearshore bars on the time scale of years: A conceptual model. Mar. Geol. 163 (1–4), 289–302. http://dx.doi.org/10.1016/s0025-3227(99)00094-8.

Sénéchal, N., Gouriou, T., Castelle, B., Parisot, J.-P., Capo, S., Bujan, S., Howa, H., 2009. Morphodynamic response of a meso- to macro-tidal intermediate beach based on a long-term data set. Geomorphology 107 (3–4), 263–274. http://dx.doi.org/10.1016/j.geomorph.2008.12.016.

Shand, R.D., Bailey, D.G., 1999. A review of net offshore bar migration with photographic illustrations from Wanganui, New Zealand. J. Coast. Res. 365–378.

Shi, F., Kirby, J.T., Harris, J.C., Geiman, J.D., Grilli, S.T., 2012. A high-order adaptive time-stepping TVD solver for Boussinesq modeling of breaking waves and coastal inundation. Ocean Model. 43–44, 36–51. http://dx.doi.org/10.1016/j.ocemod.2011.12.004.

Soulsby, R., 1997. Dynamics of Marine Sands: A Manual for Practical Applications. Thomas Telford Publications.

Soulsby, R.L., Smallman, J.V., 1986. A Direct Method of Calculating Bottom Orbital Velocity under Waves. Technical Report SR 26, Hydraulics Research Wallingford.

Splinter, K.D., Carley, J.T., Golshani, A., Tomlinson, R., 2014. A relationship to describe the cumulative impact of storm clusters on beach erosion. Coast. Eng. 83, 49–55. http://dx.doi.org/10.1016/j.coastaleng.2013.10.001.

Sunamura, T., Takeda, I., 1984. Landward migration of inner bars. Mar. Geol. 60 (1–4), 63–78. http://dx.doi.org/10.1016/0025-3227(84)90144-0.

Swart, D.H., 1974. Offshore Sediment Transport and Equilibrium Beach Profiles (Ph.D. thesis). URL https://repository.tudelft.nl/islandora/object/uuid:057cb136-5f5b-484a-878d-5616fbaeda4e.

Tătui, F., Vespremeanu-Stroe, A., Ruessink, G.B., 2016. Alongshore variability of cross-shore bar behavior on a nontidal beach. Earth Surf. Process. Landf. 41 (14), 2085–2097. http://dx.doi.org/10.1002/esp.3974.

Tucker, M.J., Pitt, E.G., 2001. Waves in Ocean Engineering. In: Elsevier Ocean Engineering Series, vol. 5, Elsevier Science.

Turner, I.L., Aarninkhof, S.G.J., Dronkers, T.D.T., McGrath, J., 2004. CZM applications of argus coastal imaging at the Gold Coast, Australia. J. Coast. Res..

van de Lageweg, W.I., Bryan, K.R., Coco, G., Ruessink, B.G., 2013. Observations of shoreline–sandbar coupling on an embayed beach. Mar. Geol. 344, 101–114. http://dx.doi.org/10.1016/j.margeo.2013.07.018.

van Enckevort, I.M.J., Ruessink, B.G., 2001. Effect of hydrodynamics and bathymetry on video estimates of nearshore sandbar position. J. Geophys. Res.: Oceans 106 (C8), 16969–16979. http://dx.doi.org/10.1029/1999jc000167.

van Enckevort, I.M.J., Ruessink, B.G., 2003. Video observations of nearshore bar behaviour. Part 1: alongshore uniform variability. Cont. Shelf Res. 23 (5), 501–512. http://dx.doi.org/10.1016/s0278-4343(02)00234-0.

Walstra, D.-J., Wesselman, D., van der Deijl, E., Ruessink, G., 2016. On the intersite variability in inter-annual nearshore sandbar cycles. J. Mar. Sci. Eng. 4 (1), 15. http://dx.doi.org/10.3390/jmse4010015.

Wijnberg, K.M., 1997. On the systematic offshore decay of breaker bars. In: Coastal Engineering 1996. American Society of Civil Engineers, pp. 3600–3613. http://dx.doi.org/10.1061/9780784402429.278.

Wijnberg, K.M., Kroon, A., 2002. Barred beaches. Geomorphology 48 (1–3), 103–120. http://dx.doi.org/10.1016/s0169-555x(02)00177-0.

Wijnberg, K.M., Terwindt, J.H., 1995. Extracting decadal morphological behaviour from high-resolution, long-term bathymetric surveys along the Holland coast using eigenfunction analysis. Mar. Geol. 126 (1–4), 301–330. http://dx.doi.org/10.1016/0025-3227(95)00084-c.

Wright, L.D., Short, A.D., 1984. Morphodynamic variability of surf zones and beaches: A synthesis. Mar. Geol. 56 (1–4), 93–118. http://dx.doi.org/10.1016/0025-3227(84)90008-2.

Zacharioudaki, A., Ravdas, M., Korres, G., 2019. Quality Information Document for the Mediterranean Sea Waves Hindcast. Published online. URL http://resources.marine.copernicus.eu/documents/QUID/CMEMS-MED-QUID-006-012.pdf.